SEDIMENTOLOGY the journal of the International Association of Sedimentologists

Sedimentology (2018) doi: 10.1111/sed.12470

Tabularity of individual turbidite beds controlled by flow efficiency and degree of confinement

QUN LIU*, BEN KNELLER*, CLAUS FALLGATTER*, VICTORIA VALDEZ BUSO* and JUAN PABLO MILANA†
*School of Geosciences, University of Aberdeen, Aberdeen AB24 3UE, UK
(Email: b.kneller@abdn.ac.uk)
†Universidad Nacional de San Juan, San Juan 5400, Argentina

Associate Editor – Jaco Baas

ABSTRACT

Submarine lobes have various geometries and stacking patterns, whose differences are likely to be the result of variations in flow efficiency and degree of confinement. This study examines four contrasting units with differing flow efficiency and confinement, to evaluate their effects on bed geometries and stacking patterns. Three of these units occur in the Late Palaeozoic Paganzo Basin, north-west Argentina: the Las Lajas system is developed in a 0·8 km wide palaeofjord; the Cerro Bola system (of which two different units were studied) was deposited in a larger sub-basin, at least 20 km wide. The Paine C system of the late Cretaceous Magallanes Basin in Chile is confined by an incision surface 3 km wide. Seventy-eight individual beds in the four units have been chosen to calculate flow efficiency and degree of confinement. Individual flow efficiency has been estimated semi-quantitatively using the outcrop cross-sectional area of the bed (as a proxy for flow volume) and percentage of mud in the beds (as a relative estimate for that in the flows). The degree of confinement experienced by the flows was assessed semi-quantitatively by dividing the flow efficiency by the maximum preserved basin dimension. It is found that: (i) degree of confinement (efficiency divided by maximum preserved basin dimension) influences individual bed geometry, highly confined flows having a higher tabularity (smaller thinning rate); (ii) in highly confined settings, individual beds stack vertically, whereas in unconfined systems, they stack compensationally; (iii) highly confined or high efficiency flows have higher tabularity (smaller thinning rate), which implies that truly sheet-like systems are only developed in highly confined and high efficiency systems. The generic model of architecture of submarine lobes and turbidite sheet systems, as a function of flow efficiency and degree of confinement, could be applied widely to sheet-like systems both at outcrop and in the subsurface.

Keywords Degree of confinement, flow efficiency, stacking patterns, submarine lobes, turbidite sheet system.

INTRODUCTION

The term submarine lobe (or splay) refers to a sediment body developed at the terminus of or lateral to a submarine channel, typically represented as having a roughly lobate, ovoid or fan-like shape (suprafan lobe and lower fan of Normark, 1970, 1978; Mutti & Normark, 1987; Pirmez *et al.*, 2000; Posamentier & Kolla, 2003). Lobes are generally considered to have broadly sheet-like internal architectures, at least as far as bed geometries can be discerned in outcrop, and

the terms 'sheet system' and 'lobe' are often used more or less interchangeably.

In this paper, the term 'submarine lobe' has been used to refer to systems in which the internal architecture is largely, if not entirely, controlled by the dynamics of the flows that build the lobe rather than any surrounding topography. The term 'turbidite sheet system' is used to refer to any turbidite depositional system where the individual beds are more or less tabular or are lenticular with very high aspect ratios (typically well in excess of 10^2). Neither term implies that the system consists wholly of turbidites, and either might include a debrite or hybrid component.

The nature of such systems has sometimes been interpreted in terms of 'flow efficiency', a qualitative concept proposed by Mutti (1979) to describe the ability of a flow to deliver sand in a basinward direction, i.e. the run-out distance. Flow efficiency is controlled by flow volume and percentage of fine-grained material in suspension (Mutti, 1992). Amy *et al.* (2000), Samuel *et al.* (2003) and Al Ja'Aidi *et al.* (2004) proposed that flow concentration also played a role.

The form of sheets or lobes may be controlled largely by the degree to which they are contained or confined by the topography. Confinement refers to the degree to which sediment gravity flows are influenced by the surrounding basin relief (Mutti & Ricci Lucchi, 1978; Thornburg *et al.*, 1990; Weaver *et al.*, 1992; Kneller, 1995; Lomas & Joseph, 2004; Smith, 2004). Confined settings can occur wherever there is negative relief on the sea floor. On large scales, they may occur in virtually any type of structurally-controlled basin, such as forearc settings (Vinnels *et al.*, 2010), foreland basins (Sinclair, 1994; Haughton, 2000; Amy *et al.*, 2007; Felletti & Bersezio, 2010), rift basins (Ravnås & Steel, 1997), intraslope salt-withdrawal basins (Winker, 1996; Prather *et al.*, 1998; Beaubouef *et al.*, 2003), and those affected by salt or shale diapirism (Van Rensbergen *et al.*, 1999). On small scales, they can occur in the relief on the top of mass-transport deposits (Armitage *et al.*, 2009; Kneller *et al.*, 2016). Whether flows are confined depends upon on their run-out distance relative to the basin size.

Various studies have suggested that apparently sheet-like turbidite systems with low flow efficiency in unconfined settings are more likely to show wedge geometry and compensational stacking architecture, i.e. individual beds are discontinuous and pinch out rather quickly in response to thickening of the underlying bed (e.g. Dudley *et al.*, 2000; Deptuck *et al.*, 2008; Jegou *et al.*, 2008; Prélat *et al.*, 2010; Marini *et al.*, 2015), whereas those systems developed in high efficiency, highly confined settings are more likely to show tabular geometries (continuous beds with a smaller rate of lateral thinning), typically showing more or less vertical stacking, without systematic offset (Haughton, 1994; Remacha & Fernández, 2003; Remacha *et al.*, 2005; Talling *et al.*, 2007a,b). However, the relationship between flow efficiency and confinement on the one hand, and stacking patterns and individual bed tabularity on the other have not yet been established.

This paper, for the first time, attempts to quantify flow efficiency and degree of confinement, and their effects on architectural styles. Detailed field data are presented from four contrasting systems in order to demonstrate the effects of these controls on spatial changes and likely lateral continuity of individual turbidite beds. Finally, a generic model is suggested for submarine lobe or sheet system architecture based on flow efficiency and degree of confinement in the system.

GEOLOGICAL CONTEXT

Geographic setting of the three field areas

The datasets are taken from three field areas (Fig. 1A). Two of the study areas (Cerro Bola and Las Lajas) are developed in the Carboniferous Paganzo Basin in north-west Argentina, in the time-equivalent Guandacol and Jejenes formations (Bashkirian; Valdez Buso *et al.*, 2017). The tectonic setting of the Paganzo Basin has been described as a retro-arc foreland basin (Ramos, 1989), a strike-slip basin (Fernández Seveso & Tankard, 1995), or half-graben (Milana *et al.*, 2010). The basin was connected by narrow seaways to the open ocean to the west, with a continental ice sheet to the east (Fig. 1B). During mid-Carboniferous times, the basin experienced several glacial events, followed by melting and consequent flooding of the continental landmass (López-Gamundí *et al.*, 1992).

The Cerro Bola area (Figs 1 and 2; Table 1), where two of the studied systems occur, is in the northern part of the basin (Fernández Seveso & Tankard, 1995; Limarino *et al.*, 2002). The sub-basin width of at least 20 km is constrained by onlap of the more distal parts of the section onto basement in the north-west, and the width of the exposed section approximately parallel to

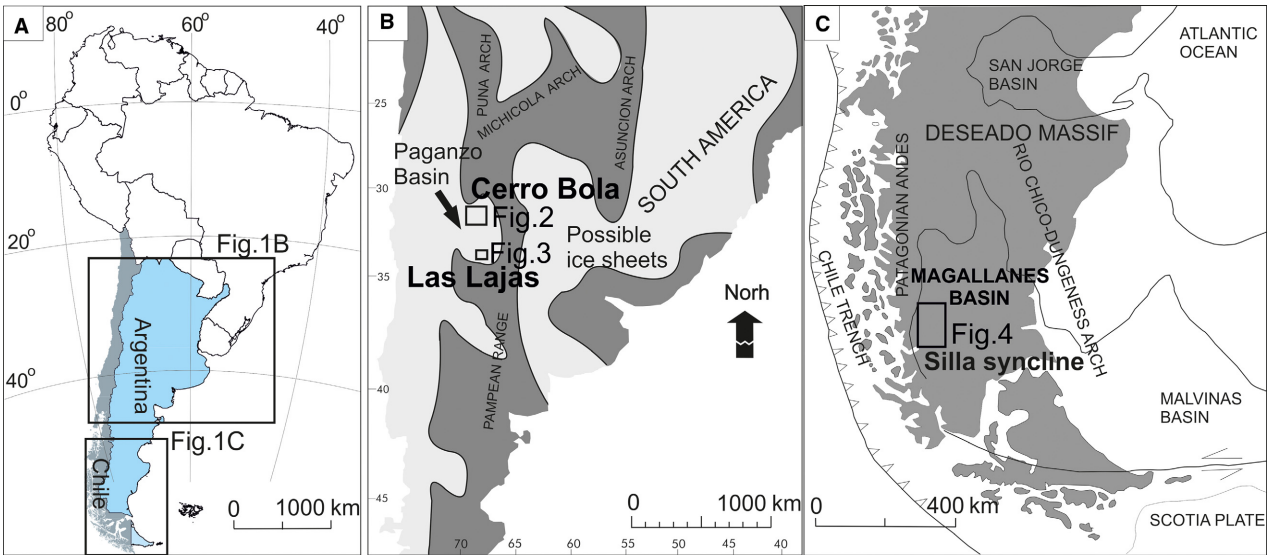

Fig. 1. (A) Geographic location of the field areas, marked as black squares. (B) Palaeogeography of the Paganzo Basin (modified from Buatois & Mángano, 1995). The Paganzo Basin was a restricted marine basin. The field localities, Cerro Bola and Las Lajas, are marked as black squares. (C) Palaeogeographic map of the Magallanes Basin (Crane & Lowe, 2008). The study area is marked as a black rectangle.

the palaeocurrents. In contrast, Las Lajas outcrops, to the SSW (Figs 1 and 3; Table 1), occur within a *ca* 1 km wide palaeofjord, incised into the Ordovician San Juan Formation limestones. The onlap onto the fjord walls is well-exposed on both sides of the fjord (Dykstra *et al.*, 2006).

The Silla syncline, is within the Magallanes Basin, located in Patagonia, southern Chile (Fig. 1C), in Torres del Paine National Park. It is regarded as part of a north–south retro-arc foreland basin (Wilson, 1983, 1991; Biddle *et al.*, 1986). The Silla syncline includes deposits of the Cerro Toro Formation (Campanian), which records the southward filling of the foreland basin (Fig. 1C; Crane & Lowe, 2008), and is interpreted here as lower to middle slope deposition. The Cerro Toro Formation is exposed as a series of generally north to south striking ridges in the fold and thrust belt east of the Andean Cordillera, and this study focuses on the exposures around the Silla syncline (Fig. 1C). The three studied outcrops therefore represent beds deposited in basins ranging in widths of over an order of magnitude (0·8 to 20 km) and within sand percentage sequences ranging by a factor of 2 (0·40 to 0·99).

Cerro Bola study area

Cerro Bola exposes an inlier of upper Palaeozoic section in a large, doubly-plunging, north–south oriented, hanging wall anticline to a thrust that dips east at about 24° (Fig. 2A; Milana *et al.*, 2010; Dykstra *et al.*, 2011) of Neogene to Recent age (Zapata & Allmendinger, 1996; Jordan *et al.*, 2001).

The succession exposed in the Cerro Bola anticline records alternations between fluviodeltaic sediments, turbidite intervals and aquatills (Dykstra *et al.*, 2011) (Fig. 2B). The overall shallowing-upward succession ranges from Carboniferous to Permian over a total stratigraphic thickness exceeding 1 km (Fig. 2B, Milana *et al.*, 2010; Dykstra *et al.*, 2011; Fallgatter *et al.*, 2017). Correlative strata occur at Sierra de Maz, *ca* 10 km to the north-west, restoring to perhaps 15 km after removal of thrust displacement (Milana *et al.*, 2010; Valdez Buso *et al.*, 2015), where Mississippian/Pennsylvanian rocks are seen to onlap metamorphic Precambrian basement, uplifted along the currently active Valle Fertil fault.

Within the Bashkirian (early Pennsylvanian), part of the Cerro Bola succession is a unit of turbidites (Milana *et al.*, 2010; Dykstra *et al.*, 2011; Fallgatter, 2015; Fallgatter *et al.*, 2017). These turbidites have been divided into five stages (named TS1 to TS5; Fig. 2; Fallgatter, 2015; Fallgatter *et al.*, 2017), of which two, TS2 and TS4 (Fig. 2B; Fallgatter *et al.*, 2017), have been chosen for detailed bed to bed correlation. The general palaeocurrent direction is towards the north-west, which means that the existing

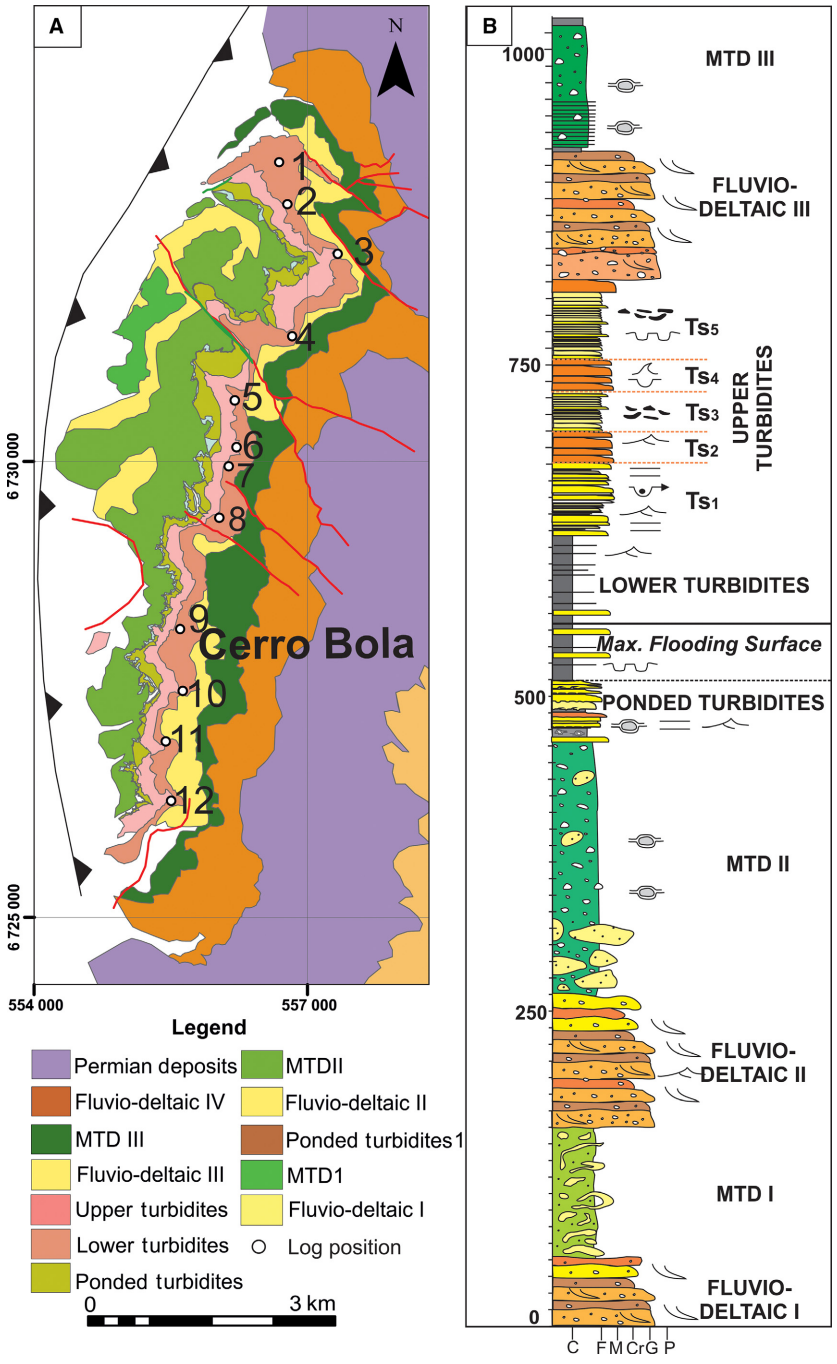

Fig. 2. (A) Geological map of Cerro Bola (after Valdez Buso *et al.*, 2015 modified from Dykstra *et al.*, 2011). (B) Stratigraphic column of Cerro Bola, represented by an alternation of fluvio-deltaic sediments, turbidite intervals and mass transport deposits (MTD): TS2 and TS4 in the Upper Turbidites interval are the subjects of this study. (Fallgatter *et al.*, 2017; modified after Milana *et al.*, 2010).

outcrop is oblique to the depositional dip direction. Both TS2 and TS4 are about 25 m in total thickness. Stage TS2 is a very sandy system, with 95% sand, whereas TS4 has 75% sand (Table 1).

Las Lajas study area

Quebrada de las Lajas, near San Juan city, western Argentina, preserves an exactly coeval Bashkirian (Valdez Buso *et al.*, 2017) glacial to post-glacial succession that was deposited in an overdeepened palaeofjord (Dykstra *et al.*, 2006) (Fig. 3A). The sedimentary succession has been divided by Dykstra *et al.* (2006) into four evolutionary stages: (i) an ice-contact delta and proglacial lake; (ii) a relatively quiet, deep-water marine environment punctuated by turbidity currents; (iii) an aggradational, confined, relatively deep-water turbidite sheet sand system; and (iv) the subaqueous portion of a progradational, coarsening and shoaling-upward coarse-

Table 1. Geological basin settings and outcrop characteristics of the four systems.

	TS2	TS4	Las Lajas	Paine C
Field area	Cerro Bola	Cerro Bola	Las Lajas	Silla syncline
Depositional setting	Subbasin	Subbasin	Palaeofjord	Confined slope
Evidence of confinement	One margin seen at outcrop, tectonic restoration suggests minimum basin width	One margin seen at outcrop, tectonic restoration suggests minimum basin width	Palaeofjord walls seen at outcrop	Bounding surface seen at outcrop
Studied Interval thickness	25 m	25 m	40 m	40 m
Orientation of outcrop	Oblique dip	Oblique dip	Oblique dip	Oblique dip
Basin width	20 km	20 km	0·8 km	3 km
Studied outcrop length	7·6 km	7·6 km	2 km	4 km
Sand (%)	95%	75%	40%	99%

grained delta (Fig. 3B). The entire sedimentary succession comprises *ca* 350 m exposed thickness (Fig. 3C), with the walls of the palaeofjord being visible at outcrop.

The studied interval is part of the stage III turbidites and is around 40 m thick, with about 40% sand. The outcrop is very well-exposed, and the individual beds chosen for the correlation in this study are virtually 100% exposed observed along the line of correlation. Three-dimensionality of the outcrop confirms the correlations.

Silla syncline study area

The Cerro Toro Formation in the Silla syncline (Fig. 4A) is at least 1100 m thick and includes three major conglomerate and sandstone units (the Pehoe, Paine and Nordenskjold members; Crane & Lowe, 2008) within a background of thin-bedded sandstone and dark grey mudstone (Fig. 4B and C). The Paine member is regarded as part of a confined slope system (Beaubouef, 2004), with an alternation of channel and lobe deposition (Crane & Lowe, 2008; Bernhardt *et al.*, 2011). The Paine Member has been divided into three sub-members, Paine A, B and C. Paine C is itself sub-divided into three phases; phases 1 and 2 represent the channel-fill, while phase 3 represents the succeeding sandy lobe (Bernhardt *et al.*, 2011) that passively infills the residual channel relief. This paper uses the term 'Paine C' to refer only to the phase 3 sandy lobe infill. This consists of an 80 m section of turbidites, confined by the erosion surface that bounds the underlying channel fill, with a width of 3 km. It is a very sandy system, with up to 99% sand. Palaeocurrents are towards the south-east, oblique to the outcrop correlated herein.

METHODS

Between the four units, eighteen sections (540 m in total) were logged at a scale of 1 : 20 to capture lithology, grain size, sedimentary structures, silt and mud percentage and bed boundaries. The correlation framework is constrained by walking bed boundaries between sections where possible, augmented with high-resolution ground-based and Unmanned aerial vehicle (drone) panoramic photomosaics. Seventy-eight individual beds are chosen and correlated in the four studied units, the smallest maximum whole bed thicknesses of which are: Paine C – 58 cm; Las Lajas – 56 cm; TS2 – 60 cm; TS4 – 90 cm. The cross-sectional area of individual beds at outcrop, A, has been used as a semi-quantitative proxy for the relative volumes of the parent flows (Talling *et al.*, 2007a,b; Malgesini *et al.*, 2015). It has been calculated using $A = 1/2 \sum_{i=1}^{n} (B_i + B_{i+1}) D_i$, where n is the number of logs that provide constraints in this study, B_n is bed thickness at log n, and D_i is the distance between successive logs in a down-current direction. Percentage of silt and mud in individual beds, P, is estimated by the thickness of silt and mud in the individual beds divided by the whole bed thickness, expressed as a percentage: $P = M_1 + M_2 + \ldots M_n / B_1 + B_2 + \ldots B_n$, where

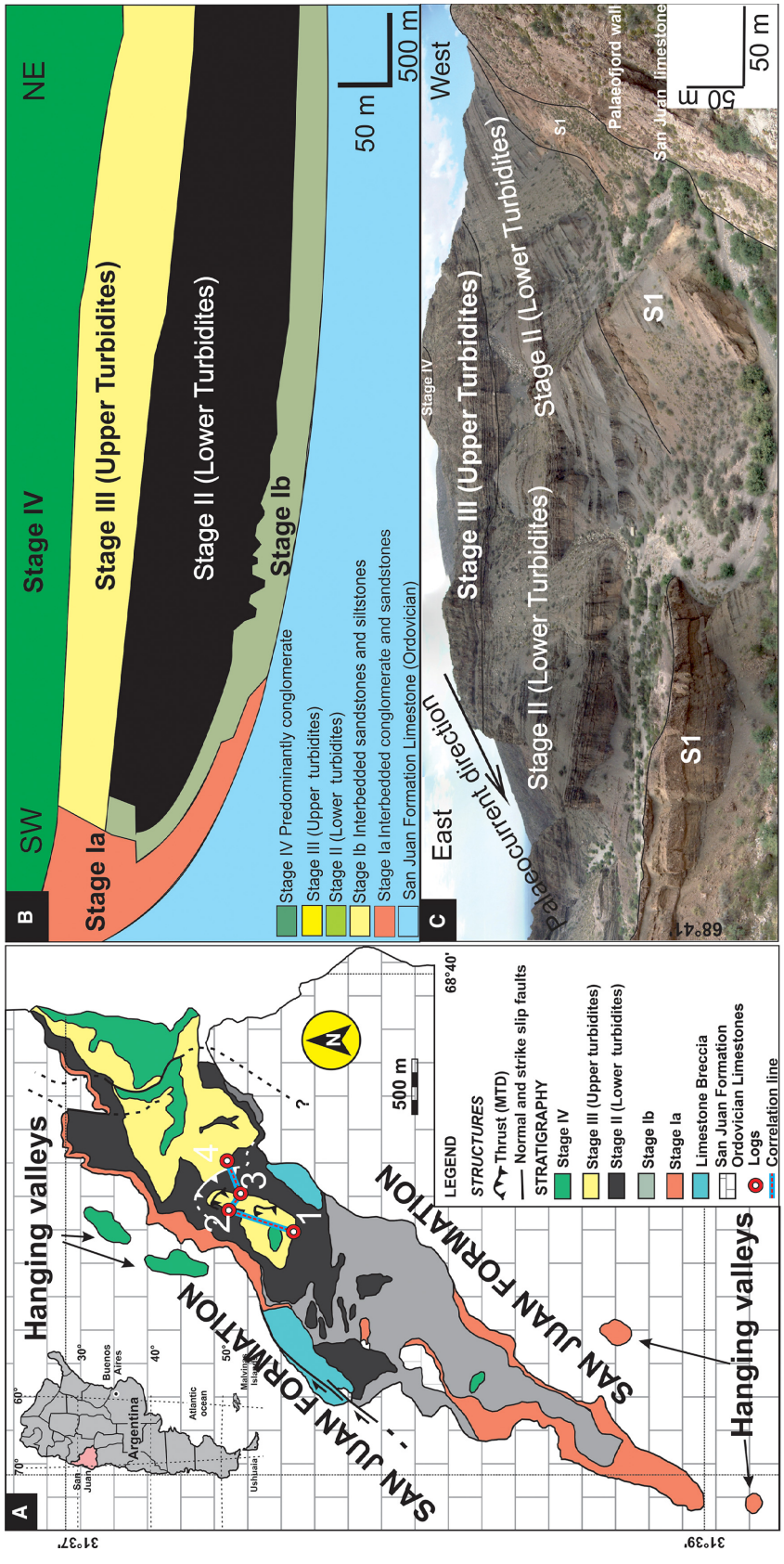

Fig. 3. (A) Geological map of Las Lajas (Fallgatter, 2015 modified after Dykstra *et al.*, 2006) with sedimentary logs undertaken in this study marked. (B) Schematic longitudinal cross-section of Las Lajas, showing the facies evolution of the palaeofjord (Dykstra *et al.*, 2006). (C) Panoramic interpretation of the entire exposed succession in Las Lajas.

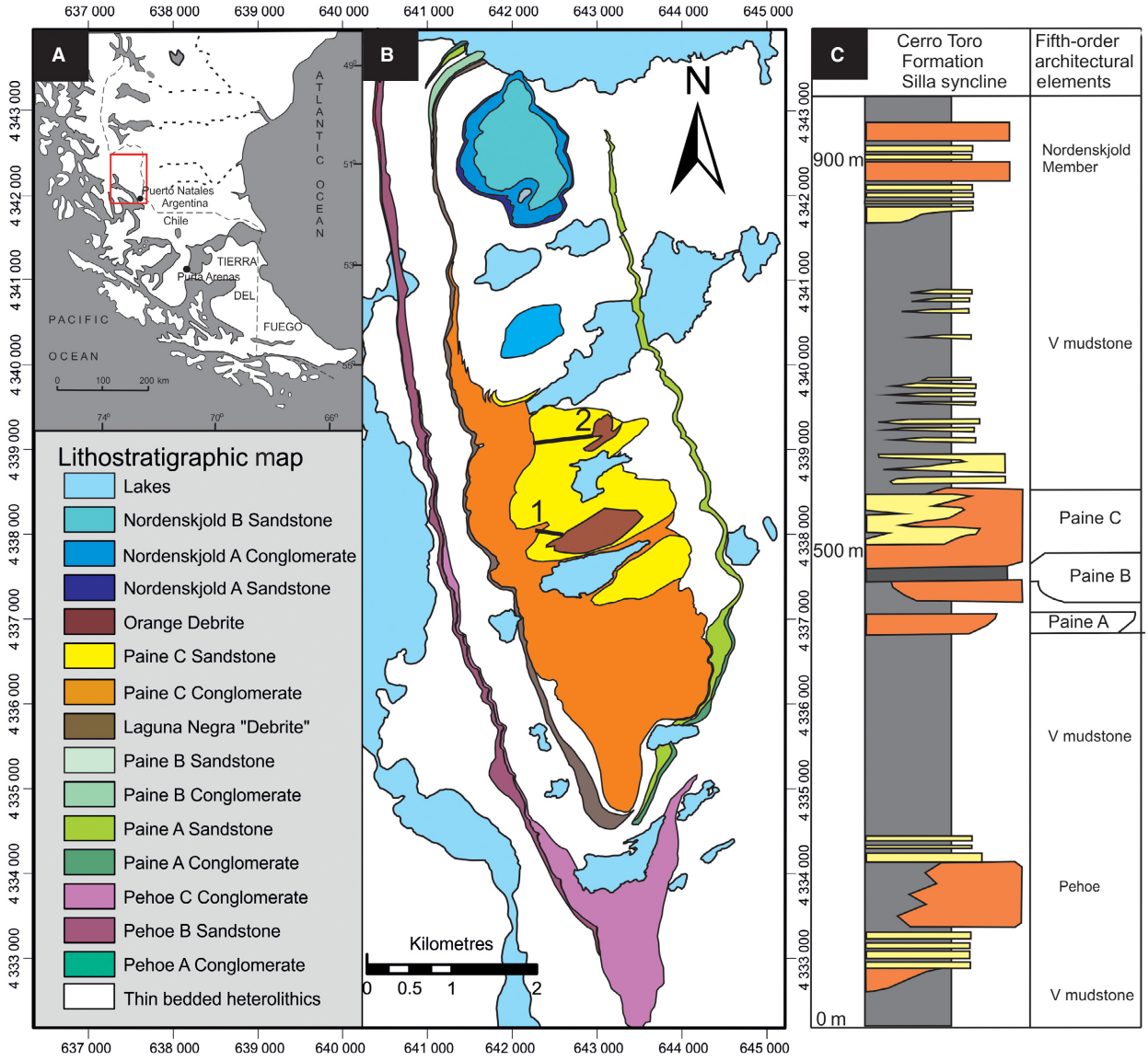

Fig. 4. (A) General location map of the study area in southern Chile. (B) Geological map of the Silla syncline showing the main units (modified from Crane & Lowe, 2008). Logged transects undertaken in this study are marked. (C) Stratigraphic column of the Cerro Toro Formation in the Silla syncline (modified from Crane & Lowe, 2008).

M_n is the mud and silt cap of an individual bed, and B_n represents the thickness of the whole bed. Although an imperfect reflection of the proportion of fine-grained material in the parent flow, it is the best proxy available for the relative proportions. Individual bed average thinning rate (%/km) in the depositional dip direction has been calculated by the bed thickness variation between the adjacent logs: $T = \sum_{i=1}^{n}(B_{i+1} - B_i)/D_i n$, where B_{i+1} and B_i are the thickness in successive logs in a down-current direction log; D_i is the distance between the two logs, and n is the number of logs taken in this study. The authors have not attempted to differentiate thin mud turbidites from the mud caps of thicker beds because this generally cannot be done reliably. Where it is possible, it is seen that the turbidite mud makes up all or almost all of the mud thickness. Thus the top of the mud cap is taken as the base of first differentiable succeeding event. This is bound to involve some error, but given the substantial thickness of the beds in question, it is argued here that the error is small and systematic. In addition, although mud may have been eroded from the top of some of the beds, especially

where sandstone beds are amalgamated, the error involved will undoubtedly be less than the observed differences between systems.

RESULTS

Individual bed characteristics of the TS2 system

System TS2 is about 25 m thick (Fig. 5A). The correlation panel goes from NNE to SSW (Fig. 5B), which is oblique to the main palaeocurrent direction (north/north-west) (Fig. 5B). The well-exposed outcrop (Fig. 5C and D) and numerous logs in the TS2 interval allow this study to capture the pinch-out of individual beds (Beds 1 to 21) along the outcrop (Fig. 5A). Individual beds wedge out along the outcrop, losing both thickness and sand percentage. Bed packages up to 8 m thick (Fig. 5C) with a mean sand thickness of 40 cm and overall sand percentage of 80%, change laterally into thin-bedded turbidites with a mean sand thickness of 5 cm, overall sand percentage of 20% and overall thickness of 5 m, over distances of about 5 km oblique to palaeocurrent (Fig. 5A).

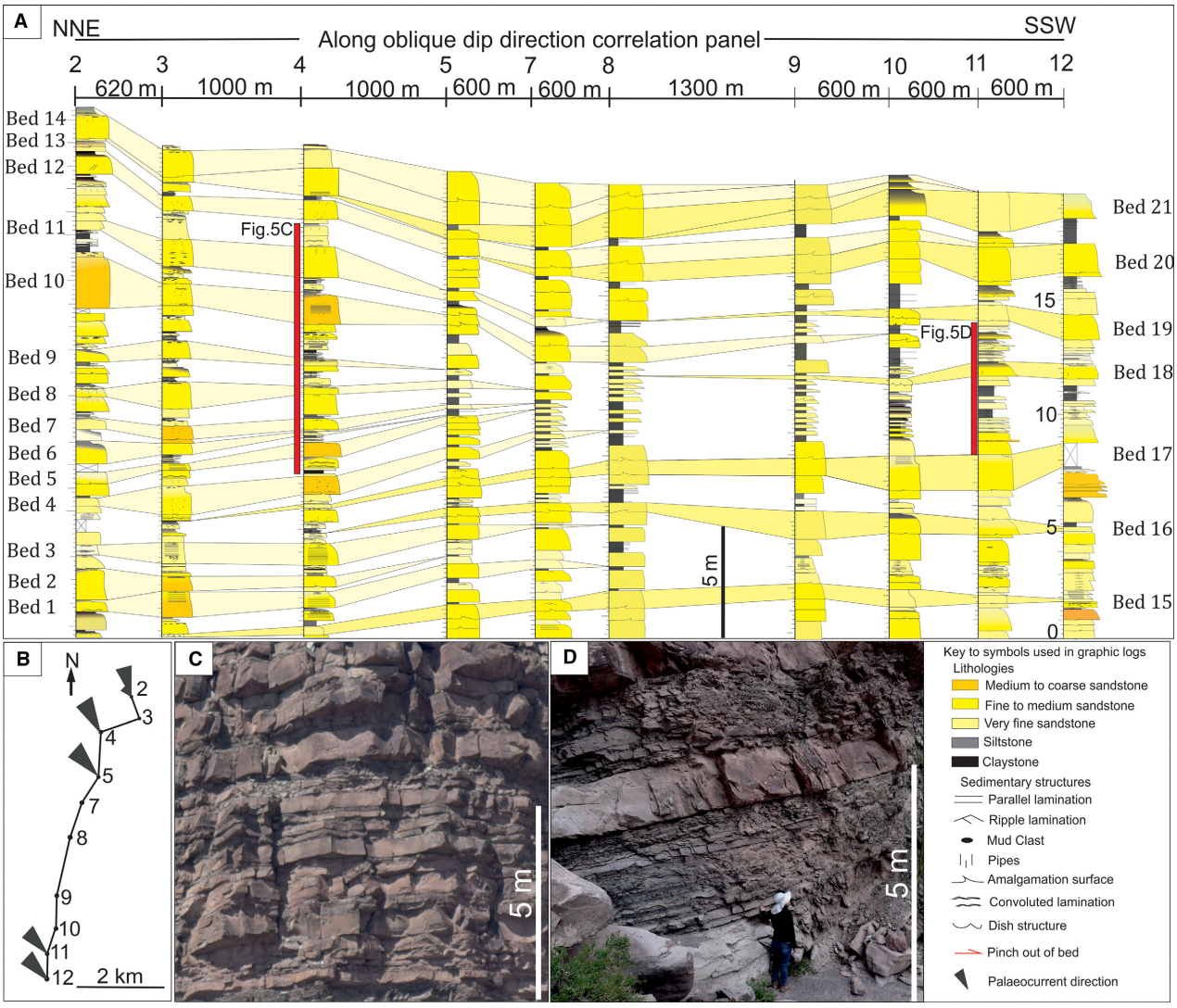

Fig. 5. (A) Correlation panel of the TS2 turbidite system. Positions of the logs are shown on (B). Individual beds (Bed 1 to Bed 21) have been correlated. (B) Field position of the sedimentary logs. The dark grey arrow represents the palaeocurrent direction measured at each position. It can be seen that the correlation section is an oblique dip direction. (C) Detailed sandstone properties of intervals logged, position showed in (A). The sand percentage is *ca* 80%. (D) Position shown in (A). The interval is dominated by thin-bedded turbidites, at the same horizon with (C).

The individual bed generally consists of a minor mud cap, constituting 2 to 5% of the whole bed thickness. The calculated average individual bed thinning rate in TS2 is 40%/km. In TS2, some individual beds (Beds 1 to 14, for instance) exhibit maximum thickness in the north, whereas some individual beds (for example, Beds 14 to 21) have their maximum thickness in the south, indicating changes in depocentre.

Individual bed characteristics of the TS4 system

The TS4 turbidite sandstones are fully exposed in a 7·6 km oblique dip direction (Fig. 6A) and they onlap basin margin basement. This restores after removal of thrust displacement (Milana *et al.*, 2010) to at least 12 km from Cerro Bola in a depositional dip direction, providing a total correlation length of *ca* 20 km. The palaeocurrents are mainly towards the north-west (Fig. 6B).

Individual beds exhibit tabular geometry (Fig. 6) and all of the larger beds (except bed 8) extend the entire length of the oblique down-current section. This contrasts with TS2, where all of the individual beds pinch out within the 7·6 km correlation panel at Cerro Bola. Also, the fact that most of the individual beds (Beds 1 to 3, 7, 9 to 11, 13 and 14) appear near the onlap implies a degree of confinement, unlike TS2, in which all the beds have pinched out before reaching the onlap.

Individual beds in TS4 always include significant mud caps, generally constituting around 30% of the total bed thickness. In general the individual beds aggrade vertically to build the whole TS4 unit.

Individual bed characteristics of the Las Lajas system

The measured turbidite interval in Las Lajas is around 40 m thick (Fig. 7A), and four logs have

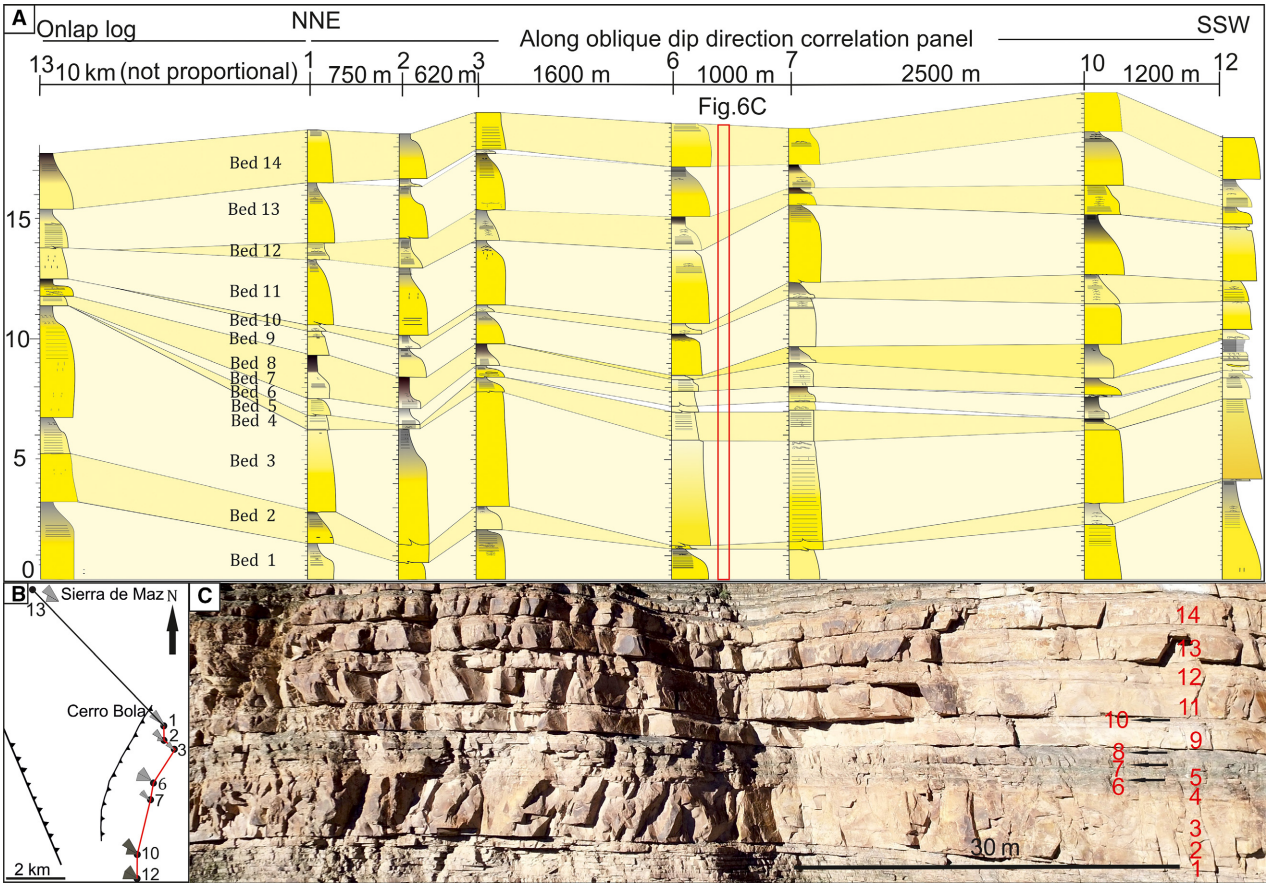

Fig. 6. (A) Correlation panel of TS4 turbidite sheet sandstone, Cerro Bola. Positions of the logs are shown on (B). Individual beds (Bed 1 to Bed 14) can be well correlated 7·6 km in oblique downdip and 12 km downdip to basin margin. (B) Locations of logs in (A), with palaeocurrent directions (marked with grey arrows). (C) Individual beds could be clearly picked out in the field because of the silty mud cap.

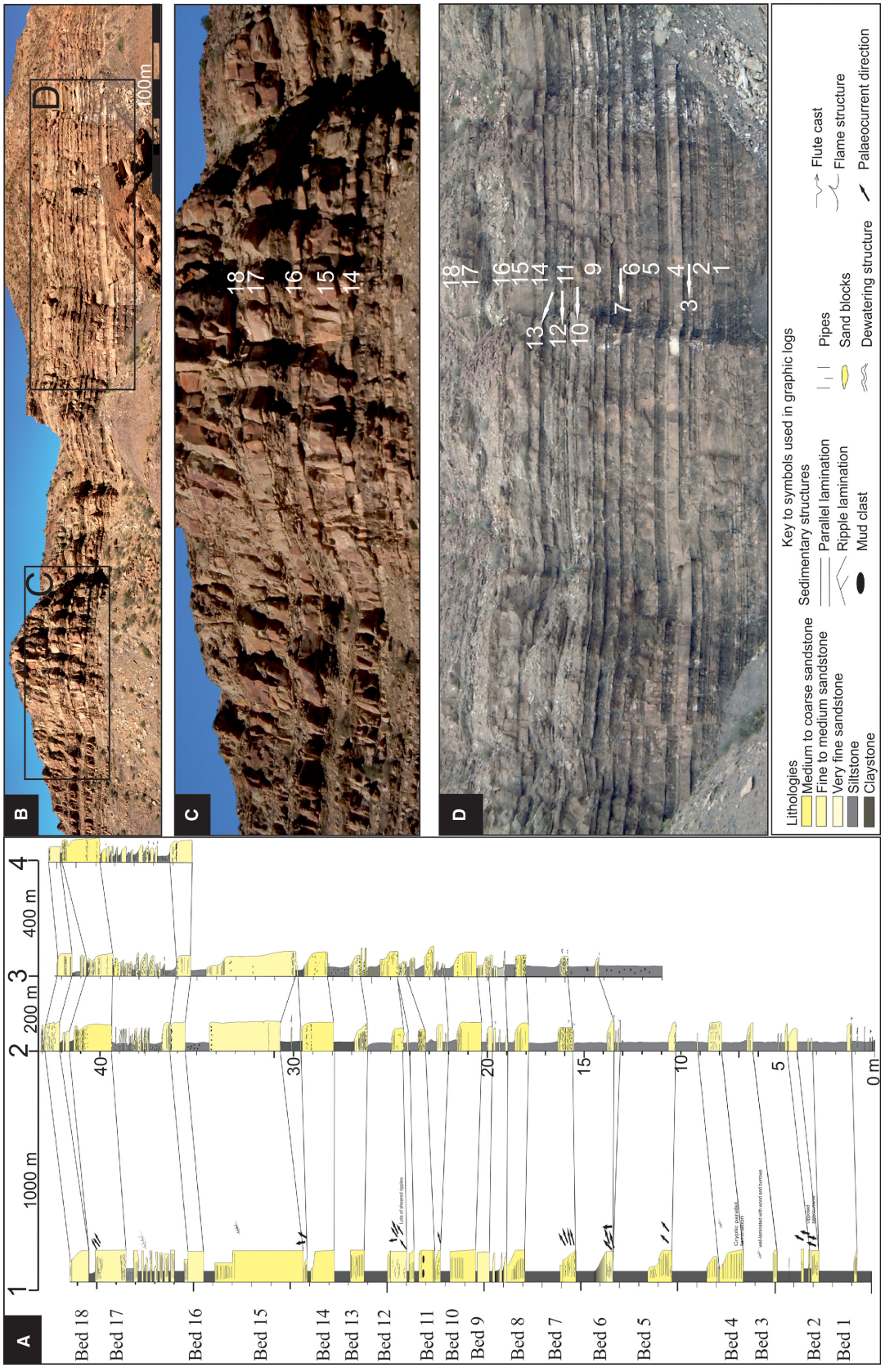

Fig. 7. (A) Correlation panel of Las Lajas turbidite sheet sandstones. Individual beds (Bed 1 to Bed 18) could be well correlated. (B) Panorama view of the Las Lajas turbidite sheet sandstones. (C) Close-up of the upper part of Las Lajas sandstone. Individual beds have mud caps. Beds (Beds 14 to 18) are labelled with numbers shown on the logs. (D) Close-up of the Las Lajas turbidite sandstone, position shown on (B). Individual beds could be picked out easily on the outcrop image and in the field. Beds are labelled with numbers shown on the logs.

been measured in a depositional dip direction. Individual beds typically have a thick mud cap (Fig. 7), indicating the high mud percentage within the flow as well as the highly confined environment which facilitates the ponding of mud. It could be seen that the individual beds (Beds 1 to 18) are tabular at a scale of 500 m (Fig. 7B), and individual beds are easily traced and correlated in the field (Fig. 7C and D).

Individual bed characteristics of the Paine C system

The Paine C turbidite sandstone interval is 32 m thick and is stratigraphically situated between underlying channel-fill conglomerates and a distinctive debrite above, which serve as good stratigraphic markers (Fig. 8A). The deposits are very sandy and highly amalgamated (Fig. 8B), and pinching out (Fig. 8C), scouring (Fig. 8D) and amalgamation of individual beds (Fig. 8E) are commonly seen in the outcrop. Amalgamation surfaces (sand–sand bed boundaries) are usually marked by granule-grade intervals (Fig. 8D). In general, the individual beds are not sheet-like even at a horizontal scale of 50 m (Fig. 8F). Twenty-five individual beds (beds that are thicker than 60 cm) have been chosen for detailed correlation (Fig. 8A).

Individual bed outcrop cross-sectional area and percentage of silt and mud

The beds in Paine C have the lowest percentage of silt and mud of the four systems studied, with a narrow range from 0·2 to 0·5% (Table 2) (Fig. 9), TS2 ranging from 2 to 5% silt and mud, TS4 ranging from 20 to 36%, while the silt and mud percentage is significantly higher in beds of Las Lajas, with a range from 34 to 76%. In order of outcrop cross-sectional area, the beds in TS4 have the largest outcrop cross-sectional area (ranging from 3680 to 30 380 m^2), averaging $1{\cdot}1 \times 10^4$ m^2; Las Lajas (from 1200 to 11 600 m^2), average $4{\cdot}1 \times 10^3$ m^2; TS2 (from 960 to 4890 m^2), average $2{\cdot}5 \times 10^3$ m^2 and, lastly, Paine C, ranging from 290 to 1340 m^2, average 6×10^2 m^2 (Table 2).

The four systems can thus be well differentiated by mean outcrop cross-sectional area of the individual beds within them, and the percentage of silt and mud (Fig. 9). The cross-sectional area of a bed at outcrop can be taken as a crude proxy for flow volume, on the assumption that bed thickness reflects flow size, and that the plan-view shape of the beds is not grossly anisotropic. The inevitable errors within these estimates are far outweighed by the differences between the various systems. Despite the caveats above, the percentage of silt and mud within a bed is the best available proxy for proportion of fines in the parent flow, although there may be a systematic bias due to ponding of mud in more confined settings (Lamb *et al.*, 2006; Marini *et al.*, 2016).

The semi-quantitative representation of flow efficiency and degree of confinement

Flow efficiency is determined by both flow volume and percentage of silt and mud in each flow. The authors have attempted to give a semi-quantitative evaluation of flow efficiency, using the simple product of bed cross-sectional area (as an approximate measure of relative flow volume) and percentage of mud and silt within the beds (as a rough measure of the relative proportions within the flows). Thus, the simple expression $E = AP$ is used (where E is flow efficiency, A is outcrop cross-sectional area, and P is percentage of silt and mud) to parameterize flow efficiency in these four systems. This assumes that flow volume and percentage of silt and mud have roughly equal effects on flow efficiency. This assumption is borne out by the experimental results of Al Ja'Aidi (2000), who showed that the increase in delivery of sediment to the basin floor was more or less equally influenced by changes in flow volume and percentage of silt and mud.

The degree of confinement in these systems is the degree to which the flows interact with the bounding topography. Since this will depend on the ability of the flows to reach the margins, it will be governed by flow efficiency, but it will also depend upon the basin size. Flows that interact with the basin margins (and may be deflected or reflected) tend to deposit beds whose geometries are controlled by those interactions (typically tabular), whereas those which are unconfined produce deposits with architectures and stacking patterns that are more likely to be self-organized. This study has evaluated confinement semi-quantitatively using the expression: $D = E/M$, where D is degree of confinement, E is flow efficiency and M is maximum preserved basin dimension. As for flow volume, this also assumes that the basins are not grossly anisotropic. Where these systems are

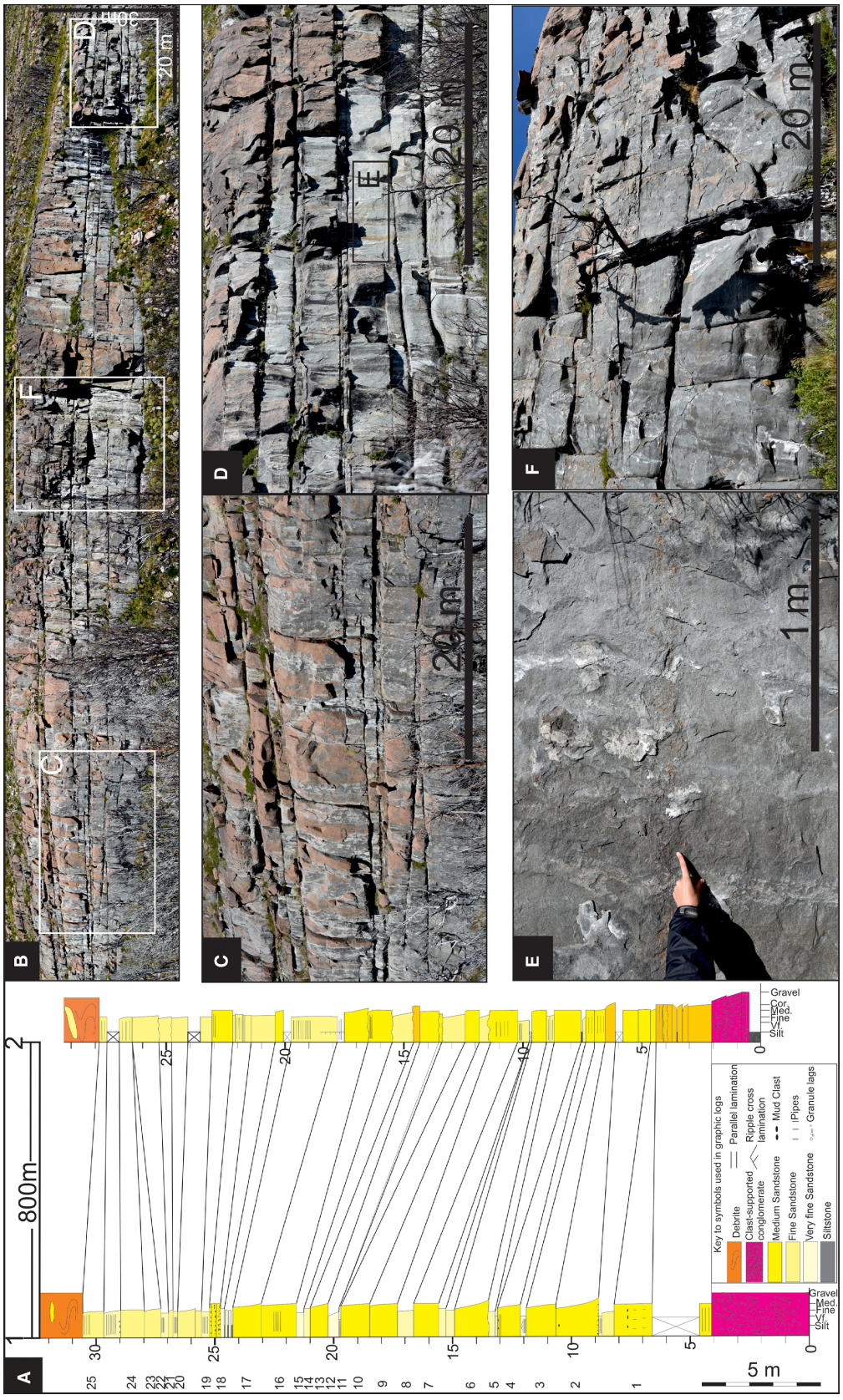

Fig. 8. (A) Correlation panel of Paine C turbidite sandstone. Individual Beds 1 to 25 have been correlated. (B) Panoramic view of the Paine C turbidite sandstone. (C) Close-up of area labelled 'C' on (B). Bed pinch out and amalgamation can be seen. (D) Close-up of area labelled 'D' on (B) 50 cm scour can be seen. (E) Close-up of (D). Bed boundaries are represented by 10 cm granule-grade intervals (indicated on figure). (F) Close-up of area labelled 'F' on (B). Packages (made up of several beds) change thickness over a distance of 20 m, showing the non-sheet-like nature of the Paine C turbidites, even at a scale of tens of metres.

Table 2. Outcrop cross-sectional area range, average outcrop cross-sectional area, percentage of silt and mud in the four systems.

	TS2	TS4	Las Lajas	Paine C
Outcrop cross-sectional area (m^2)	960 to 4890	3680 to 30 380	1200 to 11 600	290 to 1340
Average outcrop cross-sectional area (m^2)	2500	10 900	4120	600
Percentage of silt and mud	2 to 5%	20 to 36%	34 to 76%	0·2 to 0·5%

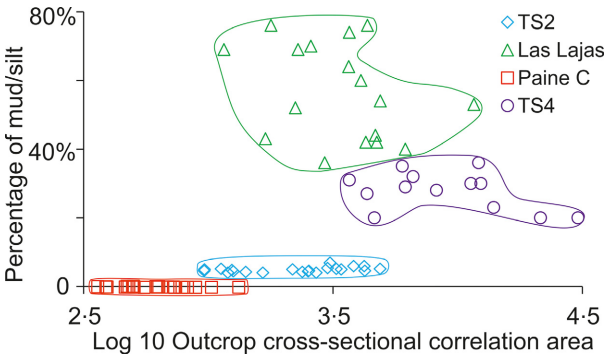

Fig. 9. Log 10 outcrop cross-sectional area against silt and mud percentage in the four systems.

in markedly elongate basins (long and laterally-confined) it raises the possibility that the stratigraphic organization may be a function of orientation, with architectures in a depositional dip direction being controlled by basin length, while the organization in a cross-stream direction is controlled by basin width.

Using the expression given above, it is found that TS4 has the highest flow efficiency ($2{\cdot}8 \times 10^3$) and Paine C the lowest (1·8), and that Las Lajas has the highest degree of confinement (2700) and Paine C the lowest (0·6) (Table 3). Thus it can be seen that the degree of confinement is not defined by absolute basin size, but by its size relative to the efficiency of the turbidite system.

Individual bed tabularity

Thinning rates (%/km), which means the percentage of bed thickness change over distances, could be best used to describe the geometry and tabularity of individual beds. Individual bed thickness decays differently in the four studied systems, i.e. exhibit different thinning rates. Taking TS2 and TS4 as examples (Fig. 10); individual beds in TS2 follow an exponential decay in thickness, while individual beds in TS4 obey a power law decay (Fig. 10), in which case, beds in TS2 generally pinch out within 4 km, and beds in TS4 only show decay in the first 3 km and maintain nearly the same thickness all the way up to the basin margin.

Table 3. Thinning rate (%/km), average flow efficiency, basin confinement and average degree of confinement in the four studied systems: TS2, TS4, Las Lajas and Paine C.

	TS2	TS4	Las Lajas	Paine C
Thinning rate (%/km)	30 to 60	5 to 23	1 to 6	45 to 100
Average thinning rate (%/km)	40	15	3	65
Average flow efficiency	76	2800	2160	1·8
Basin confinement (km)	20	20	0·8	3
Average degree of confinement	3·8	140	2700	0·6

Also, the four studied systems show large differences in average thinning rates (Fig. 11A to C; Table 3), ranging from 65%/km (Paine C), to 3%/km (Las Lajas). In other words, individual beds in Las Lajas and TS4 have much higher tabularity than TS2 and Paine C. Also, thinning rates in Paine C and TS2 are more scattered than in TS4 and Las Lajas (Fig. 11D). The increasing scatter towards the left in Fig. 11A, B and C is very likely to be the result of non-linearity of individual bed thinning rates, which becomes harder to evaluate as bed correlation lengths decrease.

Outcrop cross-sectional area and flow efficiency show negative relationships (R^2 = 0·72, 0·73) with individual bed thinning rates (%/km) in TS2, Paine C and TS4, but not in Las Lajas (Fig 11A and B). Degree of confinement shows a negative relationship (R^2 = 0·84) with thinning rates (%/km) in the four systems. Las Lajas is an

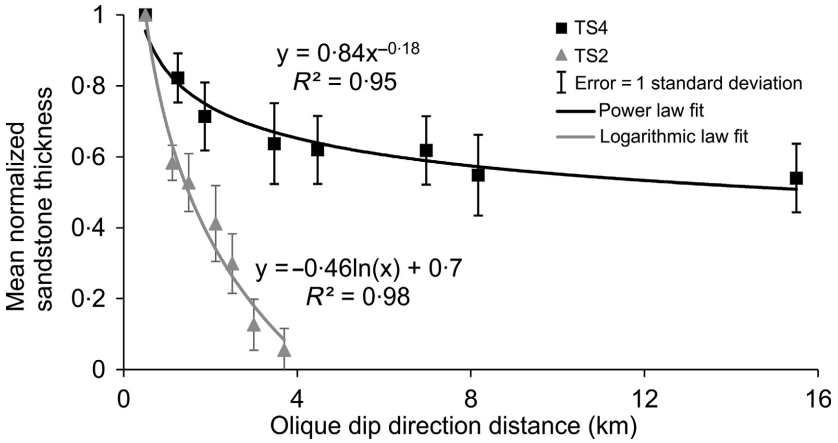

Fig. 10. Mean normalized thickness versus distance diagram for an oblique dip direction. Note that Individual beds in TS2 have an exponential decay in thickness, while individual beds in TS4 obey a power law decay.

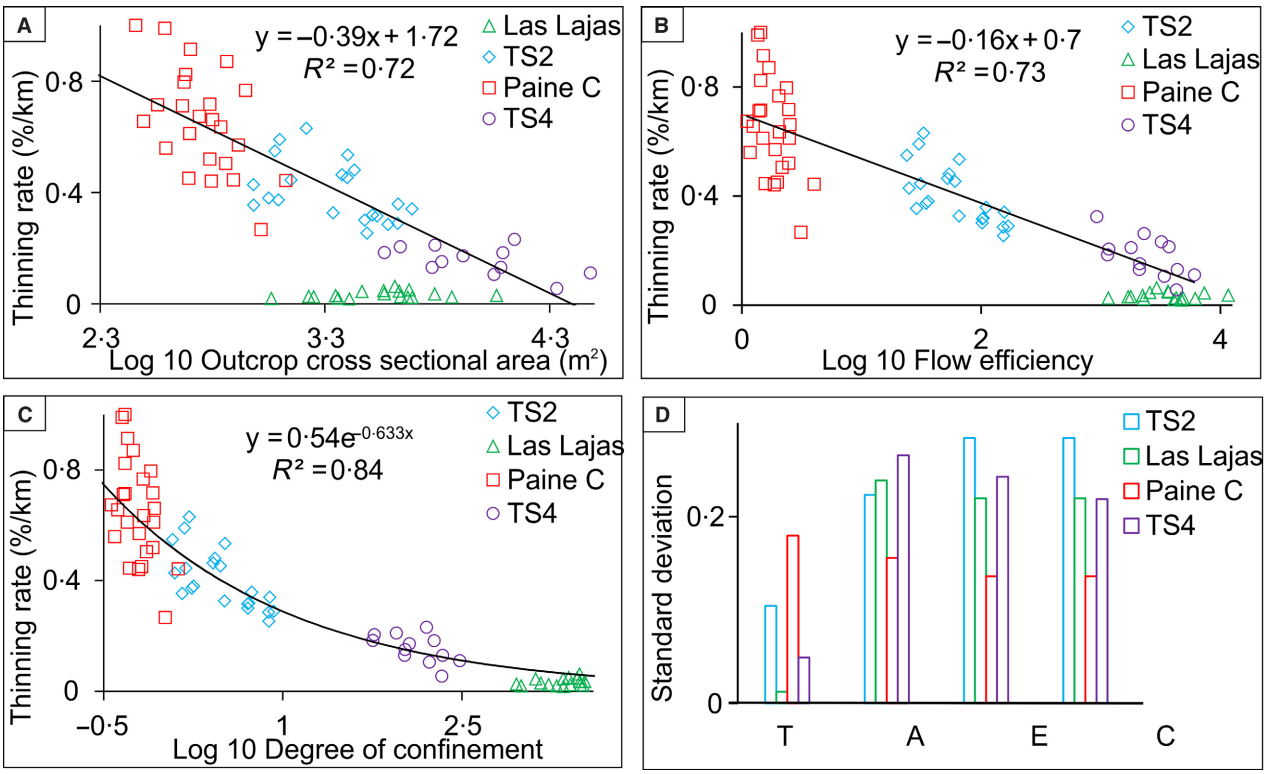

Fig. 11. (A) Scatter plots of thinning rate (%/km) versus Log 10 outcrop cross-sectional area in the four systems. (B) Scatter plots of thinning rate (%/km) versus Log 10 flow efficiency in the four systems, thinning rate in Fig 10A and B is exponential if plotted on a linear scale. (C) Scatter plots of thinning rate (%/km) versus Log 10 Degree of confinement in the four systems, note the power law best fit here, in contrast to the linear fit in Fig. 10A and B. (D) Histogram of standard deviation of: T (thinning rates); A (Log 10 outcrop cross-sectional area); E (Log 10 flow efficiency); and C (Log 10 degree of confinement).

outlier in these relationships since the cross-sectional area measurements are limited by the width of the fjord, whereas these beds probably extend for long distances in a depositional dip direction; they have thus been excluded from the best-fit calculations.

DISCUSSION

Controls on individual bed tabularity

Scatter plots of degree of confinement and flow efficiency versus thinning rate (Fig. 11B and C)

show that flow efficiency and degree of confinement play a key role in determining the individual bed depositional thickness change and thus the correlation length of individual beds. As mentioned above, flow efficiency in each system can be represented by flow size (outcrop cross-sectional area in ancient systems) and percentage of silt and mud in each system (Fig. 12A). Turbidite systems in general are quite diverse, with individual flows differing in percentage of silt and mud and in flow volume (Cossey & Kleverlaan, 1995; O'Connell *et al.*, 1995; Gorsline, 1996; Badalini *et al.*, 2000; Gorsline *et al.*, 2000; Haughton, 2000; Johnson *et al.*, 2001; Wynn *et al.*, 2002; Lien *et al.*, 2003; Hodgson & Haughton, 2004; Amy & Talling, 2006; Gervais *et al.*, 2006; Covault *et al.*, 2007; Talling *et al.*, 2007a,b; Deptuck *et al.*, 2008; Jegou *et al.*, 2008; Ducassou *et al.*, 2009; Prélat *et al.*, 2009, 2010; Etienne *et al.*, 2012; Palacios, 2012; Prather *et al.*, 2012; Picot *et al.*, 2016; Dennielou *et al.*, 2017; Fig. 12A).

It was also possible to differentiate the four systems based on the average flow efficiency and degree of confinement (Fig. 12B; Table 3): TS4 being a high efficiency, moderately confined system; Las Lajas is a moderately efficient and highly confined system; TS2 is a low efficiency, loosely confined sytem; and Paine C is a low efficiency unconfined system. The average thinning rate of these systems decreases from the low efficiency unconfined systems like Paine C (65%/km) to high efficiency highly confined systems like Marnoso Arenacea (1%/km) (Amy & Talling, 2006; Talling *et al.*, 2007a,b) and Las Lajas (3%/km) (Fig. 12B). Flow efficiency is higher in TS4 than in Peïra-Cava, but Peïra-Cava has a smaller average thinning rate (10%/km) (Amy *et al.*, 2000) than in TS4 (15%/km) due to higher degree of confinement (Fig. 12B). Flows in Peïra-Cava and Ross sandy units (Pyles, 2007) are inferred to have nearly the same flow efficiency, but in Peïra-Cava the beds show a much smaller average thinning rate than in Ross (35%/km) due to higher degree of confinement. Flows in TS4 and Ross sandy units experienced a similar degree of confinement, but beds in TS4 have smaller average thinning rates than Ross sandy units, due to a higher flow efficiency (Fig. 12B). System TS2 and Annot (Etienne *et al.*, 2012) have similar thinning rates (40%/km), with TS2 being higher in flow efficiency but less confined than Annot. Note that in all these cases the term 'unconfined' refers to individual flows and their resulting beds with respect to the bounding surfaces, and not to the geometry of the system as a whole.

The variability of individual bed thickness change rate documented in this study highlights

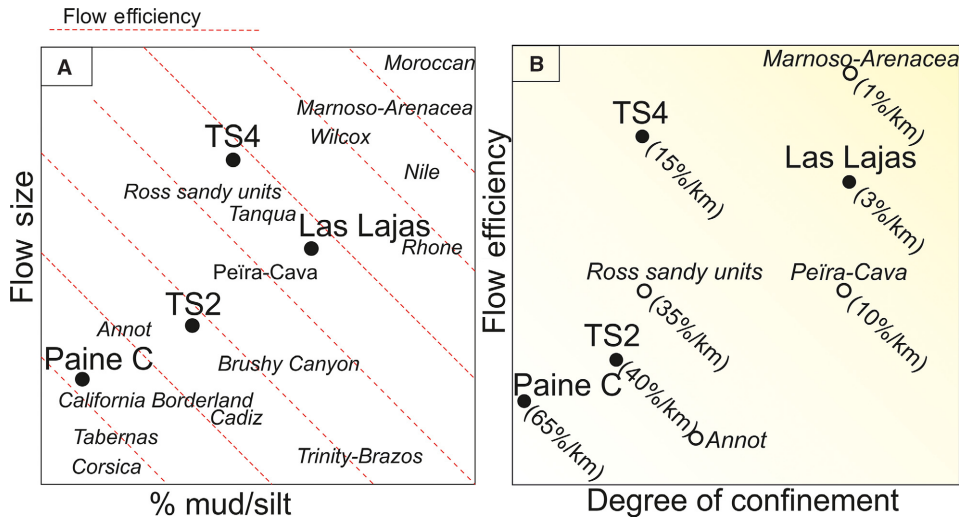

Fig. 12. (A) Simplified diagram based on actual data in this study and approximate estimates of parameters of other turbidite systems based on published data. Red dashed lines represent equal values of flow efficiency. (B) Schematic model built by combining the eight studied systems (four from this study and four from the published literature) based on flow efficiency, degree of confinement and average thinning rate. The colour gradient represents the decrease of thinning rate changing from low flow efficiency unconfined systems (bottom left corner) to high flow efficiency highly confined systems (uppermost right corner).

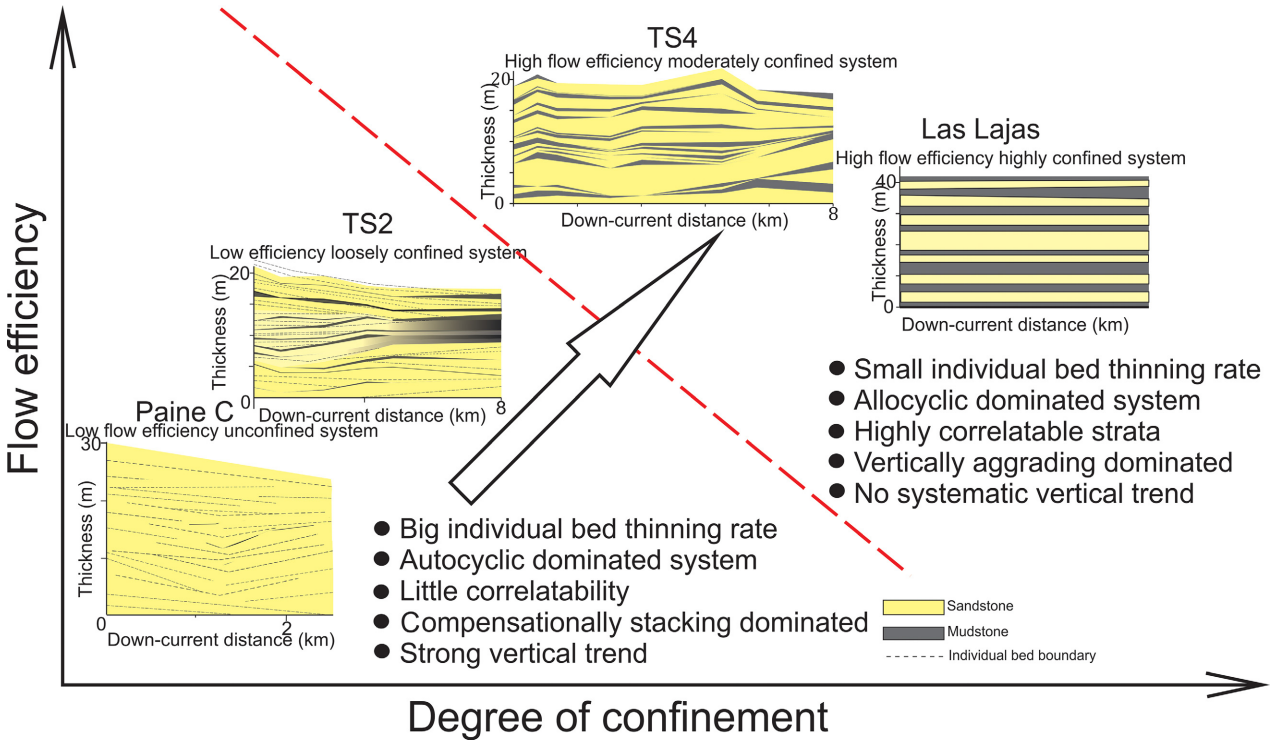

Fig. 13. Schematic cartoons showing the architecture of turbidite beds in the four systems. Paine C turbidite sandstones represent the low flow efficiency loosely confined system in which individual beds pinch out quickly. The TS2 turbidite sandstone represents the low efficiency moderately confined system in which individual beds could not be correlated for more than 2 km. There is some compensational stacking at bed scale. Las Lajas represents the moderately efficient highly confined system, in which individual beds could potentially extend tens of kilometres with little change in bed thickness. TS4 represents the high flow efficiency highly confined system, in which individual beds could potentially extend tens of kilometres without much change in bed thickness.

Table 4. Summary of the sedimentary characteristics of the four systems.

Studied interval	Paine C	TS2	Las Lajas	TS4
Represented systems	Low efficiency unconfined	Low efficiency loosely confined	Highly efficient highly confined	Highly efficient moderately confined
Individual bed thickness change rate	High	High	Low	Low
Cyclicity	Autocyclic dominated	Autocyclic dominated	Allocyclic dominated	Allocyclic dominated
Individual bed correlation confidence	Low	Low	High	High

the importance of assessing flow efficiency and degree of confinement in an unknown system. Flow efficiency could be semi-quantitatively evaluated by bed thickness, correlation length and sand percentage. Basin size could be reconstructed from seismic data. By knowing the flow efficiency and basin size of the system, a semi-quantitative estimate of degree of confinement could be obtained, which aids estimation of the thinning rate of individual beds in the system (Figs 11C and 12B).

Turbidite sheet system architecture and its controls

A simplified cartoon based on the real data has been drawn to represent the architecture of each of the four systems (Fig. 13). In Paine C, a low

efficiency and unconfined system, the sandstones have large rates of thickness change (Fig. 11). Even though the system is bounded by an erosion surface, many of the flows are so inefficient that they did not reach the margin and are thus loosely to unconfined. In TS2, a low efficiency moderately confined system, individual beds also have large rates of thickness change (Fig. 11), and individual beds pinch out into sand-poor thin-bedded turbidites before reaching the basin margin. Bed packages stack compensationally, as do individual beds in what are interpreted here as the axial parts of each package. In Las Lajas, a moderate efficiency highly confined system, individual beds have little thickness change (Fig. 11) and very high silt and mud percentages, which may in part be due to ponding. In TS4, a high efficiency highly confined system, individual beds also have a tabular character, extending all the way across the exposed part of the basin. This study recognizes that in confined systems (for example, high flow efficiency systems such as TS4 and Las Lajas; Fig. 13; Table 4), individual beds may extend across the entire basin to create basin-wide turbidite beds with low thinning rates (e.g. Sumner *et al.*, 2012; Wynn *et al.*, 2012). The turbidite beds in these systems aggrade vertically. In unconfined systems (for example, low efficiency flows in small basins) the beds have relatively higher rates of thickness change. In systems such as TS2 and Paine C, the individual beds have large rates of thickness change over short distances, so they are more likely to stack in a compensational way (e.g. Rozman, 2000).

CONCLUSIONS

This study demonstrates that the overall character of sheet-like turbidite systems is determined by a combination of factors: (i) flow efficiency, which in turn is the product of the percentage of fines within the flow, and the flow size; and (ii) the degree of confinement, which depends on the efficiency of the flows with respect to the size of the basin, the resulting architecture being dependent on flow interaction with the basin margins. For the first time, this study has attempted to quantify these parameters, using proxies that are crude and relative, but are the best available in ancient deposits. In any case, it is asserted here that the errors in these measures are likely to be smaller than the differences between distinct types of system, although they are unlikely to be an accurate reflection of small differences between similar systems.

Based on these estimates the authors note a simple correlation between these parameters and the rate of thickness decay in individual beds, which is a measure of their tabularity. Outliers from these correlations occur where the basin is small and the estimates of flow size are subject to large uncertainties (for example, due to limited outcrop length relative to the basin width or length).

These observations suggest that internal architecture of broadly sheet-like turbidite bodies – a function of flow parameters and basin size – will also determine the nature of their interactions with the basin margin, and thus their pinch-out character.

ACKNOWLEDGEMENTS

The authors would like to acknowledge the support of the PRAX 2 Joint Industry Project at the University of Aberdeen, funded by Petrochina, Statoil, BP and Det Norske (now AkerBP), which has allowed us to undertake this study. We are grateful to Professor Bryan Cronin who provided much assistance and advice in the field. We also wish to thank Jianan Wu and Guilherme Bozetti for their assistance in the field. Three reviewers (Mike Mayall, Georgios Pantopoulos and an anonymous reviewer) provided very constructive and crucial ideas, which have greatly improved the manuscript.

REFERENCES

Al Ja'Aidi, O.S. (2000) The influence of topography and flow efficiency on the deposition of turbidites. Unpublished PhD thesis. University of Leeds, UK, 162 pp.

Al Ja'Aidi, O.S., **McCaffrey, W.D.** and **Kneller, B.C.** (2004) Factors influencing the deposit geometry of experimental turbidity currents: implications for sand-body architecture in confined basins. *Geol. Soc. London Spec. Publ.*, **222**, 45–58.

Amy, L.A. and **Talling, P.J.** (2006) Anatomy of turbidites and linked debrites based on long distance (120 × 30 km) bed correlation, Marnoso Arenacea Formation, Northern Apennines, Italy. *Sedimentology*, **53**, 161–212.

Amy, L.A., **Kneller, B.** and **McCaffrey, W.D.** (2000) Evaluating the links between turbidite characteristics and gross system architecture: upscaling insights from the turbidite sheet system of Peira Cava, SE France. Deep-Water Reservoirs of the World: Houston, SEPM, Gulf Coast Section. pp. 1–15.

Amy, L.A., **Kneller, B.C.** and **McCaffrey, W.D.** (2007) Facies architecture of the Gres de Peira Cava, SE France:

landward stacking patterns in ponded turbiditic basins. *J. Geol. Soc.*, **164**, 143–162.

Armitage, D.A., **Romans, B.W.**, **Covault, J.A.** and **Graham, S.A.** (2009) The influence of mass-transport-deposit surface topography on the evolution of turbidite architecture: the Sierra Contreras, Tres Pasos Formation (Cretaceous), southern Chile. *J. Sed. Res.*, **79**, 287–301.

Badalini, G., **Kneller, B.** and **Winker, C.D.** (2000) Architecture and processes in the late Pleistocene Brazos-Trinity turbidite system, Gulf of Mexico continental slope. In: Deep-Water Reservoirs of the World: SEPM, Gulf Coast Section, 20th Annual Research Conference. pp. 16–34.

Beaubouef, R.T. (2004) Deep-water leveed-channel complexes of the Cerro Toro Formation, Upper Cretaceous, southern Chile. *AAPG Bull.*, **88**, 1471–1500.

Beaubouef, R.T., **Abreu, V.** and **Van Wagoner, J.C.** (2003) Basin 4 of the Brazos–Trinity slope system, western Gulf of Mexico: The terminal portion of a late Pleistocene lowstand systems tract. In: Shelf margin deltas and linked down slope petroleum systems: Global significance and future exploration potential: Proceedings of the 23rd Annual Research Conference, Gulf Coast Section SEPM Foundation. pp. 45–66.

Bernhardt, A., **Jobe, Z.R.** and **Lowe, D.R.** (2011) Stratigraphic evolution of a submarine channel–lobe complex system in a narrow fairway within the Magallanes foreland basin, Cerro Toro Formation, southern Chile. *Mar. Petrol. Geol.*, **28**, 785–806.

Biddle, K.T., **Uliana, M.A.**, **MitchumJr, R.M.**, **Fitzgerald, M.G.** and **Wright, R.C.** (1986) The stratigraphic and structural evolution of the central and eastern Magallanes Basin, southern South America. In: *Foreland Basins* (Eds P.A. Allen and P. Homewood), Int. Assoc. Sedimentol. Spec. Publ., **8**, 41–61.

Buatois, L.A. and **Mángano, M.G.** (1995) The palaeoenvironmental and palaeoecological significance of the lacustrine Mermia ichnofacies: an archetypical subaqueous nonmarine trace fossil assemblage. *Ichnos*, **4**, 151–161.

Cossey, S.P.J. and **Kleverlaan, K.** (1995) Heterogeneity within a sand-rich submarine fan, Tabernas Basin, Spain. In: *Atlas of Deep Water Environments* (Eds K.T. Pickering, R.N. Hiscott, N.H. Kenyon, F. Ricci-Lucchi and R.D.A. Smith), pp. 157–161. Chapman and Hall, London.

Covault, J.A., **Normark, W.R.**, **Romans, B.W.** and **Graham, S.A.** (2007) Highstand fans in the California borderland: the overlooked deep-water depositional systems. *Geology*, **35**, 783–786.

Crane, W.H. and **Lowe, D.R.** (2008) Architecture and evolution of the Paine channel complex, Cerro Toro formation (Upper Cretaceous), Silla syncline, Magallanes basin, Chile. *Sedimentology*, **55**, 979–1009.

Dennielou, B., **Droz, L.**, **Babonneau, N.**, **Jacq, C.**, **Bonnel, C.**, **Picot, M.**, **Le Saout, M.**, **Saout, Y.**, **Bez, M.**, **Savoye, B.** and **Olu, K.** (2017) Morphology, structure, composition and build-up processes of the active channel-mouth lobe complex of the Congo deep-sea fan with inputs from remotely operated underwater vehicle (ROV) multibeam and video surveys. *Deep Sea Res. Part 2 Top. Stud. Oceanogr.*, **142**, 25–49.

Deptuck, M.E., **Piper, D.J.**, **Savoye, B.** and **Gervais, A.** (2008) Dimensions and architecture of late Pleistocene submarine lobes off the northern margin of East Corsica. *Sedimentology*, **55**, 869–898.

Ducassou, E., **Migeon, S.**, **Mulder, T.**, **Murat, A.**, **Capotondi, L.**, **Bernasconi, S.M.** and **Mascle, J.** (2009) Evolution of the Nile deep-sea turbidite system during the Late Quaternary: influence of climate change on fan sedimentation. *Sedimentology*, **56**, 2061–2090.

Dudley, P.R., **Rehmer, D.E.** and **Bouma, A.H.** (2000) Reservoir-scale characteristics of fine-grained sheet sandstones, Tanqua Karoo Subbasin, South Africa. In: Deep-Water Reservoirs of the World: SEPM, Gulf Coast Section, 20th Annual Research Conference, Houston, TX. pp. 318–341.

Dykstra, M., **Kneller, B.** and **Milana, J.P.** (2006) Deglacial and postglacial sedimentary architecture in a deeply incised palaeovalley-palaeofjord—The Pennsylvanian (late Carboniferous) Jejenes Formation, San Juan, Argentina. *Geol. Soc. Am. Bull.*, **118**, 913–937.

Dykstra, M., **Garyfalou, K.**, **Kertznus, V.**, **Kneller, B.**, **Milana, J.-P.**, **Molinaro, M.**, **Szuman, M.** and **Thompson, P.** (2011) Mass-transport deposits: combining outcrop studies and seismic forward modeling to understand lithofacies distributions, deformation and their seismic expression. In: *Mass-Transport Deposits in Deepwater Settings* (Eds R.C. Shipp, P. Weimer and H.W. Posamentier), SEPM Spec., **96**, 293–310.

Etienne, S., **Mulder, T.**, **Bez, M.**, **Desaubliaux, G.**, **Kwasniewski, A.**, **Parize, O.** and **Salles, T.** (2012) Multiple scale characterization of sand-rich distal lobe deposit variability: examples from the Annot Sandstones Formation, Eocene-Oligocene, SE France. *Sed. Geol.*, **273**, 1–18.

Fallgatter, C. (2015) Confined to unconfined deep-water systems of the Paraná (Brazil) and Paganzo (Argentina) basins. PhD thesis. Universidade do Vale do Rio dos Sinos, 208 pp.

Fallgatter, C., **Kneller, B.**, **Paim, P.S.G.** and **Milana, J.P.** (2017) Transformation, partitioning and flow–deposit interactions during the run-out of megaflows. *Sedimentology*, **64**, 359–387.

Felletti, F. and **Bersezio, R.** (2010) Quantification of the degree of confinement of a turbidite-filled basin: a statistical approach based on bed thickness distribution. *Mar. Petrol. Geol.*, **27**, 515–532.

Fernández Seveso, F. and **Tankard, A.** (1995) Tectonics and Stratigraphy of the late Palaeozoic Paganzo Basin of western Argentina and its regional implications. In: *Petroleum Basins of South America* (Eds A. Tankard, S. Suarez and H.J. Welsink), AAPG Mem., **62**, 165–183.

Gervais, A., **Savoye, B.**, **Mulder, T.** and **Gonthier, E.** (2006) Sandy modern turbidite lobes: a new insight from high-resolution seismic data. *Mar. Petrol. Geol.*, **23**, 485–502.

Gorsline, D.S. (1996) Depositional events in Santa Monica Basin, California Borderland, over the past five centuries. *Sed. Geol.*, **104**, 73–88.

Gorsline, D.S., **De Diego, T.** and **Nava-Sanchez, E.H.** (2000) Seismically triggered turbidites in small margin basins: Alfonso Basin, western Gulf of California and Santa Monica Basin, California borderland. *Sed. Geol.*, **135**, 21–35.

Haughton, P.D. (1994) Deposits of deflected and ponded turbidity currents, Sorbas Basin, southeast Spain. *J. Sed. Res.*, **64**, 233–246.

Haughton, P.D. (2000) Evolving turbidite systems on a deforming basin floor, Tabernas, SE Spain. *Sedimentology*, **47**, 497–518.

Hodgson, D.M. and **Haughton, P.D.** (2004) Impact of syndepositional faulting on gravity current behaviour and deep-water stratigraphy: Tabernas-Sorbas Basin, SE Spain. *Geol. Soc. London. Spec. Publ.*, **222**, 135–158.

Jegou, I., **Savoye, B.**, **Pirmez, C.** and **Droz, L.** (2008) Channel-mouth lobe complex of the recent Amazon Fan: the missing piece. *Mar. Geol.*, **252**, 62–77.

Johnson, S.D., **Flint, S.**, **Hinds, D.** and **De Ville Wickens, H.** (2001) Anatomy, geometry and sequence stratigraphy of basin floor to slope turbidite systems, Tanqua Karoo, South Africa. *Sedimentology*, **48**, 987–1023.

Jordan, T.E., **Schlunegger, F.** and **Cardozo, N.** (2001) Unsteady and spatially variable evolution of the Neogene Andean Bermejo foreland basin, Argentina. *J. S. Am. Earth Sci.*, **14**, 775–798.

Kneller, B. (1995) Beyond the turbidite paradigm: physical models for deposition of turbidites and their implications for reservoir prediction. *Geol. Soc. London. Spec. Publ.*, **94**, 31–49.

Kneller, B., **Dykstra, M.**, **Fairweather, L.** and **Milana, J.P.** (2016) Mass-transport and slope accommodation: implications for turbidite sandstone reservoirs. *AAPG Bull.*, **100**, 213–235.

Lamb, M.P., **Toniolo, H.** and **Parker, G.** (2006) Trapping of sustained turbidity currents by intraslope minibasins. *Sedimentology*, **53**, 147–160.

Lien, T., **Walker, R.G.** and **Martinsen, O.J.** (2003) Turbidites in the Upper Carboniferous Ross Formation, western Ireland: reconstruction of a channel and spillover system. *Sedimentology*, **50**, 113–148.

Limarino, C.O., **Césari, S.N.**, **Net, L.I.**, **Marenssi, S.A.**, **Gutierrez, R.P.** and **Tripaldi, A.** (2002) The Upper Carboniferous postglacial transgression in the Paganzo and Rıo Blanco basins (northwestern Argentina): facies and stratigraphic significance. *J. S. Am. Earth Sci.*, **15**, 445–460.

Lomas, S.A. and **Joseph, P.** (2004) Confined turbidite systems. *Geol. Soc. London. Spec. Publ.*, **222**, 1–7.

López-Gamundí, O.R., **Limarino, C.O.** and **Cesari, S.N.** (1992) Late Palaeozoic palaeoclimatology of central west Argentina. *Palaeogeogr. Palaeoclimatol. Palaeoecol.*, **91**, 305–329.

Malgesini, G., **Talling, P.J.**, **Hogg, A.J.**, **Armitage, D.**, **Goater, A.** and **Felletti, F.** (2015) Quantitative analysis of submarine-flow deposit shape in the Marnoso-Arenacea Formation: what is the signature of hindered settling from dense near-bed layers? *J. Sed. Res.*, **85**, 170–191.

Marini, M., **Milli, S.**, **Ravnås, R.** and **Moscatelli, M.** (2015) A comparative study of confined vs. semi-confined turbidite lobes from the Lower Messinian Laga Basin (Central Apennines, Italy): implications for assessment of reservoir architecture. *Mar. Petrol. Geol.*, **63**, 142–165.

Marini, M., **Felletti, F.**, **Milli, S.** and **Patacci, M.** (2016) The thick-bedded tail of turbidite thickness distribution as a proxy for flow confinement: examples from tertiary basins of central and northern Apennines (Italy). *Sed. Geol.*, **341**, 96–118.

Milana, J.P., **Kneller, B.** and **Dykstra, M.** (2010) Mass-transport deposits and turbidites, syn-to-post-glacial carboniferous basins of Western Argentina. ISC 2010F Guid, 01-88.

Mutti, E. (1979) Turbidites et cones sous-marins profonds. In: *Sédimentation Détritique (Fluviatile, Littorale et Marine)*, vol. **1** (Ed. P. Homewood), pp. 353–419. Institut Géologique Université de Switzerland, Fribourg.

Mutti, E. (1992) Turbidite sandstones. Agip, Istituto di geologia, Università di Parma.

Mutti, E. and **Normark, W.R.** (1987) Comparing examples of modern and ancient turbidite systems: problems and concepts. In: *Marine Clastic Sedimentology* (Eds J.K. Legget and G.G. Zuffa), pp. 1–38. Springer, The Netherlands.

Mutti, E. and **Ricci Lucchi, F.** (1978) Turbidites of the northern Apennines: introduction to facies analysis. *Int. Geol. Rev.*, **20**, 125–166.

Normark, W.R. (1970) Growth patterns of deep-sea fans. *AAPG Bull.*, **54**, 2170–2195.

Normark, W.R. (1978) Fan valleys, channels, and depositional lobes on modern submarine fans: characters for recognition of sandy turbidite environments. *AAPG Bull.*, **62**, 912–931.

O'Connell, S., **McHugh, C.** and **Ryan, W.B.F.** (1995) Unique fan morphology in an entrenched thalweg channel on the Rhone Fan. In: *Atlas of Deep Water Environments* (Eds K.T. Pickering, N. Hiscott, R. Smith and N.H. Kenyon), pp. 80–83. Springer, The Netherlands.

Palacios, Z. (2012) Climate change as a controlling parameter in sediment supply: the Nile province. PhD thesis, University of Aberdeen.

Picot, M., **Droz, L.**, **Marsset, T.**, **Dennielou, B.** and **Bez, M.** (2016) Controls on turbidite sedimentation: insights from a quantitative approach of submarine channel and lobe architecture (Late Quaternary Congo Fan). *Mar. Petrol. Geol.*, **72**, 423–446.

Pirmez, C., **Beaubouef, R.T.**, **Friedmann, S.J.** and **Mohrig, D.C.** (2000) Equilibrium profile and base level in submarine channels: examples from Late Pleistocene systems and implications for the architecture of deepwater reservoirs. In: Global deep-water reservoirs: Gulf Coast Section SEPM Foundation 20th Annual Bob F. Perkins Research Conference. pp. 782–805.

Posamentier, H.W. and **Kolla, V.** (2003) Seismic geomorphology and stratigraphy of depositional elements in deep-water settings. *J. Sed. Res.*, **73**, 367–388.

Prather, B.E., **Booth, J.R.**, **Steffens, G.S.** and **Craig, P.A.** (1998) Classification, lithologic calibration, and stratigraphic succession of seismic facies of intraslope basins, deep-water Gulf of Mexico. *AAPG Bull.*, **82**, 701–728.

Prather, B.E., **Pirmez, C.A.R.L.O.S.** and **Winker, C.D.** (2012) Stratigraphy of linked intraslope basins: Brazos-Trinity system western Gulf of Mexico. Application of the Principles of Seismic Geomorphology to Continental Slope and Base-of-Slope Systems: case Studies from Seafloor and Near-Seafloor Analogues. *SEPM Spec. Publ.*, **99**, 83–110.

Prélat, A., **Hodgson, D.M.** and **Flint, S.S.** (2009) Evolution, architecture and hierarchy of distributary deepwater deposits: a highresolution outcrop investigation from the Permian Karoo Basin, South Africa. *Sedimentology*, **56**, 2132–2154.

Prélat, A., **Covault, J.A.**, **Hodgson, D.M.**, **Fildani, A.** and **Flint, S.S.** (2010) Intrinsic controls on the range of volumes, morphologies, and dimensions of submarine lobes. *Sed. Geol.*, **232**, 66–76.

Pyles, D.R. (2007) Architectural elements in a ponded submarine fan, Carboniferous Ross Sandstone, western Ireland. In: *Atlas of Deep-water Outcrops* (Eds T.H. Nilsen, R.D. Shew, G.S. Steffens and J.R.J. Studlick), AAPG Studies in Geology, **56**, 206–209.

Ramos, V.A. (1989) Andean foothills structures in northern Magallanes Basin, Argentina. *AAPG Bull.*, **73**, 887–903.

Ravnås, R. and **Steel, R.J.** (1997) Contrasting styles of Late Jurassic syn-rift turbidite sedimentation: a comparative study of the Magnus and Oseberg areas, northern North Sea. *Mar. Petrol. Geol.*, **14**, 417–449.

Remacha, E. and **Fernández, L.P.** (2003) High-resolution correlation patterns in the turbidite systems of the Hecho Group (South-Central Pyrenees, Spain). *Mar. Petrol. Geol.*, **20**, 711–726.

Remacha, E., **Fernández, L.P.** and **Maestro, E.** (2005) The transition between sheet-like lobe and basin-plain turbidites in the Hecho basin (south-central Pyrenees, Spain). *J. Sed. Res.*, **75**, 798–819.

Rozman, D.J. (2000) Characterization of a fine-grained outer submarine fan deposit, Tanqua-Karoo basin, South Africa. In: *Fine-Grained Turbidite Systems* (Eds A.H. Bouma and J. Stone), AAPG Mem., **72**, 291–298.

Samuel, A., **Kneller, B.**, **Raslan, S.**, **Sharp, A.** and **Parsons, C.** (2003) Prolific deep marine slope channels of the Nile Delta, Egypt. *AAPG Bull.*, **87**, 541–560.

Sinclair, H.D. (1994) The influence of lateral basinal slopes on turbidite sedimentation in the Annot sandstones of SE France. *J. Sed. Res.*, **64**, 42–54.

Smith, R.U. (2004) Silled sub-basins to connected tortuous corridors: sediment distribution systems on topographically complex sub-aqueous slopes. *Geol. Soc. London. Spec. Publ.*, **222**, 23–43.

Sumner, E.J., **Talling, P.J.**, **Amy, L.A.**, **Wynn, R.B.**, **Stevenson, C.J.** and **Frenz, M.** (2012) Facies architecture of individual basin-plain turbidites: comparison with existing models and implications for flow processes. *Sedimentology*, **59**, 1850–1887.

Talling, P.J., **Amy, L.A.**, **Wynn, R.B.**, **Blackbourn, G.** and **Gibson, O.** (2007a) Evolution of turbidity currents deduced from extensive thin turbidites: Marnoso Arenacea Formation (Miocene), Italian Apennines. *J. Sed. Res.*, **77**, 172–196.

Talling, P.J., **Amy, L.A.** and **Wynn, R.B.** (2007b) New insight into the evolution of large-volume turbidity currents: comparison of turbidite shape and previous modelling results. *Sedimentology*, **54**, 737–769.

Thornburg, T.M., **Kulm, L.D.** and **Hussong, D.M.** (1990) Submarine-fan development in the southern Chile Trench: a dynamic interplay of tectonics and sedimentation. *Geol. Soc. Am. Bull.*, **102**, 1658–1680.

Valdez Buso, V., **Milana, J.P.** and **Kneller, B.** (2015) Megadeslizamientos gravitacionales de la Formación Guandacol en Cerro Bola y Sierra de Maz y su relación con la glaciación del Paleozoico Tardío, La Rioja, Argentina. *Lat. Am. J. Sedimentol. Basin Anal.*, **22**, 109–133.

Valdez Buso, V., **di Pasquo, M.**, **Milana, J.P.**, **Kneller, B.**, **Fallgatter, C.**, **Chemale Junior, F.** and **Paim, P.** (2017) Integrated U-Pb zircon and palynological/palaeofloristic age determinations of a Bashkirian palaeofjord fill, Quebrada Grande (Western Argentina). *J. S. Am. Earth Sci.*, **73**, 202–222.

Van Rensbergen, P., **Morley, C.K.**, **Ang, D.W.**, **Hoan, T.Q.** and **Lam, N.T.** (1999) Structural evolution of shale diapirs from reactive rise to mud volcanism: 3D seismic data from the Baram delta, offshore Brunei Darussalam. *J. Geol. Soc. London*, **156**, 633–650.

Vinnels, J.S., **Butler, R.W.H.**, **Mccaffrey, W.D.** and **Paton, D.A.** (2010) Depositional processes across the Sinu Accretionary Prism, offshore Colombia. *Mar. Petrol. Geol.*, **27**, 794–809.

Weaver, P.P.E., **Rothwell, R.G.**, **Ebbing, J.**, **Gunn, D.** and **Hunter, P.M.** (1992) Correlation, frequency of emplacement and source directions of megaturbidites on the Madeira Abyssal Plain. *Mar. Geol.*, **109**, 1–20.

Wilson, T.J. (1983) Stratigraphic and structural evolution of the Ultima Esperanza foreland fold-thrust belt, Patagonian Andes, southern Chile. Doctoral dissertation, Columbia University.

Wilson, T.J. (1991) Transition from back-arc to foreland basin development in the southernmost Andes: stratigraphic record from the Ultima Esperanza District, Chile. *Geol. Soc. Am. Bull.*, **103**, 98–111.

Winker, C.D. (1996) High-resolution seismic stratigraphy of a Late Pleistocene submarine fan ponded by salt-withdrawal mini-basins on the Gulf of Mexico continental slope. Proceedings from 1996 Offshore Technology Conference, Paper OTC 8024, May 6-9, 1996, Houston, TX. pp. 619–628.

Wynn, R.B., **Weaver, P.P.**, **Masson, D.G.** and **Stow, D.A.** (2002) Turbidite depositional architecture across three interconnected deep-water basins on the north-west African margin. *Sedimentology*, **49**, 669–695.

Wynn, R.B., **Talling, P.J.**, **Masson, D.G.**, **Le Bas, T.P.**, **Cronin, B.T.** and **Stevenson, C.** (2012) The influence of subtle gradient changes on deep-water gravity flows: a case study from the Moroccan turbidite system. *SEPM Spec. Publ.*, **99**, 371–383.

Zapata, T.R. and **Allmendinger, R.W.** (1996) Growth stratal records of instantaneous and progressive limb rotation in the Precordillera thrust belt and Bermejo basin, Argentina. *Tectonics*, **15**, 1065–1083.

Manuscript received 22 November 2017; revision accepted 22 February 2018